Electronic structure, surface states, surface energy, and work function of the Cu(100) surface

H. Bross
Sektion Physik, Universität München, Theresienstrasse 37, 80333 München, Germany and Department of Physics, Montana State University, Bozeman, Montana 59715

M. Kauzmann
Sektion Physik, Universität München, Theresienstrasse 37, 80333 München, Germany
(Received 4 October 1994; revised manuscript received 30 January 1995)

The modified augmented-plane-wave (MAPW) method is adapted for film geometry. Emphasis is especially put on the choice of the trial functions to achieve high accuracy for the Bloch state as well as for the self-consistent potential in the local-density approximation. Results obtained for one-, three-, five-, and seven-layer Cu(100) films are found to be in good qualitative agreement with other investigations. However, a more precise comparison with recent investigations shows some deviations which are outside the range of accuracy characteristic for a method. At $\overline{X}$ and $\overline{M}$ surface states are found which are more or less close to the experimental results. The density of states and the electronic charge in the middle of the seven-layer film are only slightly different from the corresponding magnitudes in the bulk evaluated by use of the MAPW method with similar computational parameters. With increasing number of layers the work function approaches the margin of the experimental values. As the total energy of the films turns out to be proportional to the number of layers a reasonable value of the surface energy could be given. For the electric field gradient a value was obtained which is by about a factor of 3 smaller than its experimental value. This is due to the fact that in the present calculation the effective potential is assumed to be spherical within the muffin-tin spheres.

I. INTRODUCTION

Theoretically, the (100) surface of transition and noble metals has been investigated intensively. Almost all methods originally developed for calculating the band structure of the bulk have been adapted to films. Without being complete, this includes the pseudopotential plane-wave method,[1] the linear combination of atomic orbitals (LCAO) method,[2–6] the linearized augmented-plane-wave (LAPW) method,[7–13] the full-potential linearized-augmented-plane-wave (FLAPW) method,[14–16] the linear combination of Gaussian-type orbitals fitting-function (LCGTO-FF or FILMS) method,[17,18] and the film linearized muffin-tin orbital (FLMTO) method.[19] The early investigations[4,7,8] were based on heuristic potentials obtained either from bulk energy bands or by superposing relativistic atomic charge densities. Most self-consistent calculations were performed with muffin-tin potentials inside the film and a potential varying only in the direction perpendicular to the surface. Great progress has been achieved since the advent of the FLAPW method,[14] which like the LCGTO-FF method[17,18] allows for a potential without any shape approximations. At present both methods are considered to be standard for high-precision studies of surfaces.[16] Thus very surprisingly their applications to a Cu(100) monolayer by Birkenheuer *et al.*[20] gave energies of some occupied states that differ by up to 18 mRy and for the Fermi energy by 27 mRy. These deviations are outside the margin of error characteristic for either method, say 3 mRy, and are not small with regard to the width of d bands in Cu. They demonstrate that at least one scheme is less accurate. Therefore it is desirable to repeat these investigations using a scheme which allows for even higher accuracy. The adaption of the modified augmented-plane-wave (MAPW) scheme[21–24] to the film problem fits well for this purpose. Analogously to the FLAPW and the FILMS schemes, it is a linear method but it is more flexible with respect to the trial functions used to solve the eigenvalue problem. By an appropriate choice of parameters characteristic for the basis set, any degree of accuracy can be achieved. In addition, the solutions of the eigenvalue problem are continuous and differentiable everywhere and all eigenstates obtained by this scheme are orthogonal to one another. No shape restriction of the potential is necessary.

The second goal of the present investigation is to check to what extent the electronic structure in the middle of a film of moderate thickness is comparable with that of the bulk. If such a comparison turns out to be satisfactory the electronic structure near the boundaries of the film and the surface of a semi-infinite medium having the same crystal structure will be comparable, too. This would be a very important result since up to now, with some exceptions,[25,26] no self-consistent calculations have been published where the surface matching problem has been treated in the sense described in the pioneering work of Appelbaum and Hamann,[27] which requires

that both the oscillating and the evanescent Bloch waves corresponding to a certain wave vector parallel to the surface have to be considered. Steps in this direction[25,28,29] have been made. But, for example, in the surface embedding method self-consistency of the electronic structure is obtained only for the upper two layers.

II. FORMALISM

As in the film LMTO method[7] and the film LAPW method,[8] all space is partioned into three regions: (1) touching muffin-tin (MT) spheres, centered on each nucleus, (2) the interstitial region between the spheres, and (3) the vacuum region (Fig. 1). As we have two-dimensional translation symmetry the film is constructed by a periodic repetition in space of an identical structural unit. Within the (100) film this unit consists of an oblique column which is generated by repeating the Wigner-Seitz cell along the principal lattice vector $\vec{a}_3$. Its domain is defined by

$$\Omega_c = \left\{ \vec{r} \,|\, \vec{r} = \sum_{i=1}^{3} t_i \vec{a}_i, \quad |t_1| \le \frac{1}{2}, \ |t_2| \le \frac{1}{2}, \ |t_3| \le \frac{d}{a} \right\}, \quad (1)$$

where $\vec{a}_i$ are the primitive lattice vectors

$$\vec{a}_1 = \frac{a}{2}(1,1,0), \ \vec{a}_2 = \frac{a}{2}(1,-1,0), \ \vec{a}_3 = \frac{a}{2}(0,1,1). \quad (2)$$

d denotes the distance between the boundary planes and a is the lattice constant. The area of the two-dimensional Wigner-Seitz cell is $A = |a_1 \times a_2| = a^2/2$ and the volume of the column is $V_c = dA$.

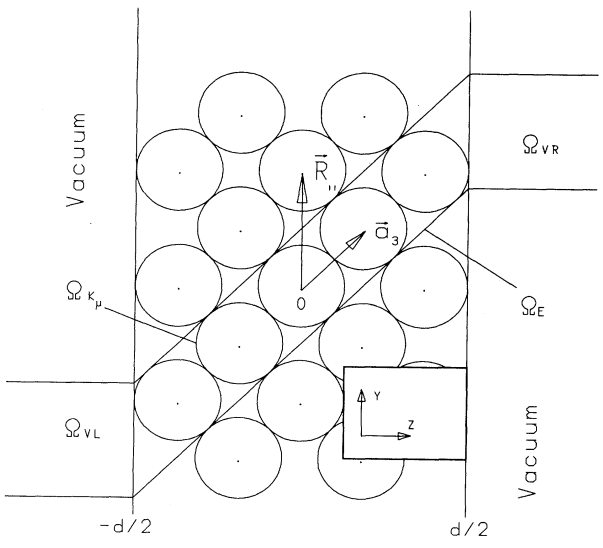

FIG. 1. Schematic representation of the (001) film geometry. The unit column indicated by full lines extends to $z = \pm\infty$. There are two boundary planes at $z = \pm d/2$.

This partioning has the advantage that the radius of the MT spheres has the same value, $a/\sqrt{8}$, as in the bulk. In most other investigations[7,8] a perpendicular column is used with the result that the radius of the MT sphere is considerable smaller, $a/4$. Then in all APW-like schemes additional plane waves are necessary to describe the wave functions outside the MT spheres. Outside the film, as in other treatments, a perpendicular column is used on both sides.

A considerable reduction of the numerical work is achieved by considering (100) films with an odd number of layers only. Thus we have both inversion and mirror symmetry with respect to the plane $z = 0$, where the z axis is chosen in the direction perpendicular to the surface. No specific shape approximation of the potential is assumed in the following treatment. But in the course of the numerical work the potential is taken to be spherically symmetric inside the MT sphere. In the case of close-packed metals this shape restriction of the potential has no significant influence on most physical properties.

This section describes the choice of the trial functions used to solve the extremal problem of the Schrödinger equation and the construction of the charge density and of the effective potential as well as the evaluation of the total energy in the local-density approximation (LDA).[30]

A. The basis functions

1. *Interstitial region*

In the interstitial region a basis function is defined, as in the LAPW scheme, as a product of a two-dimensional plane wave having the correct two-dimensional Bloch behavior and a one-dimensional symmetrized plane wave,

$$\langle \vec{r} \,|\, \vec{k}_{||} + \vec{K}_{||}, p_l, \pm \rangle = e^{i(\vec{k}_{||}+\vec{K}_{||})\cdot\vec{r}_{||}} \times \begin{cases} \cos(p_l z) & (+) \\ \sin(p_l z) & (-). \end{cases} \quad (3)$$

Here $\vec{r}_{||}$ and z are the components of $\vec{r}$ parallel and perpendicular to the surface, respectively. + and − denote states which are, respectively, symmetric and antisymmetric with respect to z reflection. $\vec{k}_{||}$ is a two-dimensional crystal momentum vector and $\vec{K}_{||}$ is a two-dimensional reciprocal lattice vector. In order to obtain trial functions of great flexibility p_l is defined by

$$p_l = l \frac{2\pi}{\lambda d}, \quad l = 0,1,2,\ldots . \quad (4)$$

If we choose $\lambda > 1$ these trial functions or their derivatives with respect to z will not have a node at the boundary. In their LAPW scheme Krakauer *et al.*[8] saw this point as they decided to test the effect by choosing $\lambda > 1$ in future calculations. The optimal value of λ is found by requiring that the energy eigenvalues of the occupied states remain almost stationary with respect to a variation of λ. From Table I we learn that this value depends sensitively on the number of layers. With these basis functions the wave function in the whole film is given by the superposition

TABLE I. Optimal values of λ according to Eq. (4).

	λ
Monolayer	2.828
Three layers	1.500
Five layers	1.375
Seven layers	1.300

$$\psi_{\vec{k}_{||},\pm}(\vec{r}) = \frac{1}{\sqrt{V_c}} \sum_{\vec{K}_{||}} \sum_{p_l} v(\vec{K}_{||}, p_l) \langle \vec{r} \,|\, \vec{k}_{||} + \vec{K}_{||},\ p_l,\ \pm \rangle. \tag{5}$$

V_c is the volume of the elementary column within the film. The summation in Eq. (5) extends over a finite number of $\vec{K}_{||}$'s and p_l's (see Sec. III).

2. *Muffin-tin sphere*

As a result of the strong Coulomb singularity the wave function $\psi_{\vec{k}_{||},\pm}(\vec{r})$ shows strong variations near the nuclei. Therefore we augment it, in the MT sphere centered at $\vec{R}^\mu = \mu \vec{a}_3$, $\mu = -(N-1)/2, \ldots, (N)/2$, in the central elementary column of the N-layer slab by the additional sum

$$\delta\psi^{\mu}_{\vec{k}_{||},\pm}(\vec{r}) = \frac{1}{\sqrt{V_c}} \sum_{l=0}^{L} (2l+1) i^l Y_{lm}(\vec{r}'_0)\, P^{\mu,\pm}_{lm}(r'), \tag{6}$$

where

$$\begin{aligned} P^{\mu,\pm}_{lm}(r') = {} & \sum_s A^{\mu}_{slm} R^{\mu}_{sl}(r') - \frac{1}{1 + i \pm (1-i)} \sum_{\vec{K}_{||}} \sum_{p_l} v(\vec{K}_{||}, p_l) \\ & \times \Big[e^{i(\vec{k}_{||}+\vec{K}_{||}+p_l \vec{e}_z)\cdot\vec{R}^\mu} Y^*_{lm}([\vec{k}_{||} + \vec{K}_{||} + p_l \vec{e}_z]^0)\ j_l(|\vec{k}_{||} + \vec{K}_{||} + p_l \vec{e}_z| r') \\ & \pm e^{i(\vec{k}_{||}+\vec{K}_{||}-p_l \vec{e}_z)\cdot\vec{R}^\mu} Y^*_{lm}([\vec{k}_{||} + \vec{K}_{||} - p_l \vec{e}_z]^0)\ j_l(|\vec{k}_{||} + \vec{K}_{||} - p_l \vec{e}_z| r') \Big] \end{aligned} \tag{7}$$

and

$$\vec{r}\,' = \vec{r} - \vec{R}^\mu. \tag{8}$$

Unit vectors are denoted by the superscript 0. Y_{lm} are real spherical harmonics and j_l are spherical Bessel functions. The radial functions R^μ_{sl} are the regular solutions of the radial differential equation

$$\frac{d^2 R^\mu_{sl}}{dr^2} + \frac{2}{r}\frac{dR^\mu_{sl}}{dr} - \frac{l(l+1)}{r^2} R^\mu_{sl} - V^\mu(r)\, R^\mu_{sl} + E^\mu_{sl}\, R^\mu_{sl} = 0\ . \tag{9}$$

V^μ is the spherical potential within the MT sphere located at $\vec{R}^\mu$ which generally changes from layer to layer. To get a linear eigenvalue problem the energies E^μ_{sl} are determined by requiring that the logarithmic derivative $(dR^\mu_{sl}/dr)/R^\mu_{sl}$ at the surface of the MT sphere be either $+1$ or -1. The index $s = 1, 2, \ldots$ counts these solutions. The sums over $\vec{K}_{||}$ and p_l subtracted in Eq. (7) are nothing else but the angular decomposition of the plane-wave expansion (5) up to L. That means for $l \le L$ the $\psi_{\vec{k}_{||},\pm}(r)$ consists of products of the radial functions R^μ_{sl} and spherical harmonics. In contrast to the usual APW scheme the angular decomposition of the plane waves (5) gives products of spherical harmonics and spherical Bessel functions for $L < l < \infty$.

3. *The exterior or vacuum region*

The basic function in the vacuum region is defined as a product of a two-dimensional plane wave, as in the interstitial region, and a z dependent function. In order to achieve a maximum amount of freedom for the wave functions near the boundaries the z-dependence is described by the so-called B splines.[31] For that purpose $N+5$ distinct points are defined with

$$z_{-3} < z_{-2} < z_{-1} < \frac{d}{2} = z_0 < z_1 \cdots z_N < z_{N+1}, \tag{10}$$

which are assumed quadratically spaced around the boundary $z = z_0 = d/2$ and

$$z_n = d/2 + (z_N - d/2)\ n^2/N^2\ . \tag{11}$$

A B spline $S_\tau(z)$ consists of piecewise cubic polynomials which are only nonzero on the support $[z_{\tau-2}, z_{\tau+2}]$ and is normalized by requiring $S_\tau(z_{\tau-2}) = 1$.

Then a basis function in the vacuum region is defined by

$$\langle \vec{r} \,|\, \vec{k}_{||} + \vec{K}_{||}\ , \tau \rangle = \frac{1}{\sqrt{V_c}}\, e^{i(\vec{k}_{||}+\vec{K}_{||})\cdot\vec{r}_{||}} S_\tau(z)\ , \qquad \tau = 1, \ldots, N+1. \tag{12}$$

As the basis function with $\tau = N+1$ shows too strong a decay for $z > z_N$ we define

$$\langle \vec{r} \,|\, \vec{k}_{||} + \vec{K}_{||}, N+1 \rangle = \alpha\, e^{i(\vec{k}_{||}+\vec{K}_{||})\cdot\vec{r}}\ e^{\beta(z-z_N)} \tag{13}$$

for $z \ge z_{N+1}$, where α and β are determined by requiring that the basis function and its first derivative be continuous at $z = z_N$. Note that the points z_{-3}, z_{-2}, and z_{z-1} as well as z_{N+1} have no physical meaning. They have only been introduced to have a unique definition of the B splines at the boundaries. The splines with $4 \le \tau \le N$ are called inner splines as they are zero for $z \le d/2$ and

$z \geq z_N$. For an optimal choice of the parameters N and z_N see Sec. III. The expansion coefficients of such a basis function will be denoted by $w(\vec{K}_{||}, \tau)$. In the following it will turn out to be advantageous that the trial function consists only of finite sums. Thus no special considerations are necessary to check their convergence.

B. The eigenvalue problem

1. Constraints guaranteeing the continuity of the wave function

As in the MAPW scheme[21,22] we require that the wave function be continuous and differentiable everywhere. On the surface of the MT sphere we have

$$P^{\mu}_{lm}(r^{\mu}_{\mathrm{APW}}) = 0 \quad \text{and} \quad \frac{dP^{\mu}_{lm}}{dr}(r^{\mu}_{\mathrm{APW}}) = 0,$$

$$l \leq L, \quad |m| \leq L, \quad (14)$$

for $\mu = -(N-1)/2, \ldots, (N-1)/2$ in the case of an N-layer slab.

On the boundary $z = d/2$ each two-dimensional plane wave within the slab joins continuously to the two-dimensional plane wave in the exterior if we set

$$\sum_{p_l} v(\vec{K}_{||}, p_l) \cos(p_l\, d/2) = \sum_{\tau=1}^{3} w(\vec{K}_{||}, \tau)\, S_{\tau}(d/2), \quad (15)$$

$$-\sum_{p_l} v(\vec{K}_{||}, p_l)\, p_l \sin(p_l\, d/2) = \sum_{\tau=1}^{3} w(\vec{K}_{||}, \tau) \frac{dS_{\tau}}{dz}(d/2) \quad (16)$$

in the case of even solutions. In the case of odd solutions the sine and cosine are to be interchanged and the minus sign on the left side of Eq. (16) is to be omitted. Equations (14), (15), and (16) guarantee the eigenvalue problem to be Hermitian. In total the number of constraints as a result of the requirement of continuity is given by

$$N_{\mathrm{constr}} = 2\left[N(L+1)^2 + N_{\mathrm{PW}}\right], \quad (17)$$

where N_{PW} is the number of two-dimensional plane waves.

2. Variational principle

We proceed in the usual manner and make the expectation value of the energy stationary under the constraints of normalization and continuity of the wave function and its first derivative, as described by Eqs. (14)–(16). These conditions are incorporated by means of Lagrangian multipliers $-E$, α^{μ}_{lm}, β^{μ}_{lm}, $\gamma_{\vec{K}_{||}}$, and $\delta_{\vec{K}_{||}}$. After a lengthy but straightforward calculation (for details, see Ref. 32) we arrive at a secular equation which has the following form:

$$\begin{pmatrix} \underline{H}_{11} & \underline{H}_{12} & 0 & & \\ \underline{H}_{21} & \underline{H}_{22} & 0 & \underline{c}_1^{+}\ \underline{c}_2^{+}\ \underline{c}_3^{+}\ \underline{c}_4^{+} & \\ 0 & 0 & \underline{H}_{33} & & \\ & \underline{c}_1 & & & \\ & \underline{c}_2 & & 0 & \\ & \underline{c}_3 & & & \\ & \underline{c}_4 & & & \end{pmatrix} \begin{pmatrix} \underline{v} \\ \underline{A} \\ \underline{w} \\ \underline{\alpha} \\ \underline{\beta} \\ \underline{\gamma} \\ \underline{\delta} \end{pmatrix}$$

$$= E \begin{pmatrix} \underline{\lambda}_1 & 0 & 0 & & & & \\ 0 & \underline{\lambda}_2 & 0 & & & & \\ 0 & 0 & \underline{\lambda}_3 & & & & \\ & & & 0 & & & \\ & & & & 0 & & \\ & & & & & 0 & \\ & & & & & & 0 \end{pmatrix} \begin{pmatrix} \underline{v} \\ \underline{A} \\ \underline{w} \\ \underline{\alpha} \\ \underline{\beta} \\ \underline{\gamma} \\ \underline{\delta} \end{pmatrix}, \quad (18)$$

where the submatrices $\underline{H}_{ij}$ generate the matrix element $\langle \psi \,|\, H \,|\, \psi \rangle$, the $\underline{\lambda}_i$ guarantee the normalization of ψ, and finally where the $\underline{c}_i$ force the wave function to be continuous and differentiable everywhere. The vectors $\underline{v}$, $\underline{A}$, $\underline{w}$, $\underline{\alpha}$, $\underline{\beta}$, $\underline{\gamma}$, and $\underline{\delta}$ are shorthand notation for the expansion coefficients $v(\vec{K}_{||}, p_l)$, A^{μ}_{slm}, $w(\vec{K}_{||}, \tau)$, and for the Lagrange parameters α^{μ}_{lm}, β^{μ}_{lm}, $\gamma_{\vec{K}_{||}}$, and $\delta_{\vec{K}_{||}}$. H_{12} and H_{21} are zero in the case of spherically symmetric warped muffin-tin (WMT) potentials which are not restricted outside the MT spheres. Explicit expressions for $\underline{H}_{ij}$, $\underline{\lambda}_i$, and $\underline{c}_i$ have been given by one of the authors.[32]

Equation (18) is a linear Hermitian eigenvalue problem. As described in Ref. 22 a reduction of the rank of the eigenvalue problem is possible without destroying the Hermiticity by eliminating twice as many equations as the vector of Lagrange parameters α^{μ}_{lm}, β^{μ}_{lm}, $\gamma_{\vec{K}_{||}}$, and $\delta_{\vec{K}_{||}}$ has components. The remaining eigenvalue problem is solved by use of standard Hermitian eigenvalue routines, e.g., by NAG, EISPACK, or IMSL, yielding for fixed value of $\vec{k}_{||}$ all possible eigenfunctions simultaneously. Due to the Hermiticity any two nondegenerate solutions are orthogonal to one another within numerical accuracy. That means even orthogonality between core and highly excited valence states is fulfilled exactly. In this respect the present formulation is superior to the LAPW method where orthogonality is only guaranteed for energies lying in a certain energy range of about 1 Ry.

C. The electronic charge density

The evaluation of the electronic charge density according to the Kohn-Sham[30] scheme is straightforward, but lengthy. For details, see again Ref. 32. At the end we find that within the film it consists of two terms,

$$\rho(\vec{r}) = \rho^{\mathrm{I}}(\vec{r}) + \rho^{\mathrm{II}}(\vec{r}). \quad (19)$$

The first, ρ^{I}, comes from the superposition of plane waves according to Eq. (5) and may be regrouped in the following way

$$\rho^{\mathrm{I}}(\vec{r}) = \sum_{\vec{K}_{||}} \rho^{\mathrm{I}}_{\vec{K}_{||}}(z)\, S_{\vec{K}_{||}}(\vec{r}_{||}). \quad (20)$$

$S_{\vec{K}_{||}}(\vec{r}_{||})$ denotes a linear combination of two-dimensional plane waves invariant under the symmetry operations of the point group which leaves the atoms of the film invariant, e.g., the group C_{4V} in the case of the (100) layer.[33] $\rho^{\mathrm{I}}_{\vec{K}_{||}}$ is a superposition of circular cosine-functions with amplitudes obtained by summing over the $\vec{k}_{||}$ vectors of the irreducible wedge and over different bands according to their occupancy.

The contribution $\rho^{\mathrm{II}}(\vec{r})$ is only nonzero within MT spheres. It originates from the square of the P^{μ}_{lm}'s and the cross products of the P^{μ}_{lm}'s with the plane waves. By help of the lattice harmonics $K_{lm}(\vec{r}^{\,0})$ we get

$$\rho^{\mathrm{II}}(\vec{r}) = \sum_{\mu=-(N-1)/2}^{(N-1)/2} \Theta\left(r^{\mu}_{\mathrm{APW}} - r'\right) \times \sum_{l=0,m}^{\infty} \rho^{\mu}_{lm}(r')\, K_{lm}\left(\vec{r}^{\,\prime 0}\right), \quad \vec{r}' = \vec{r} - \vec{R}^{\mu}, \tag{21}$$

with the Heaviside step function Θ.

Again the density of multipole moments $\rho^{\mu}_{lm}(|\vec{r}-\vec{R}^{\mu}|)$ is obtained by summing over the $\vec{k}$ vectors of the irreducible wedge and over the different bands according to their occupancy. The most leading moments are characterized by the angular moments $l \leq 2L$ with L as defined in (6). $\rho^{\mathrm{II}}(\vec{r})$ also contains contributions from the core states which have been omitted in the eigenvalue problem. In each iteration this contribution has been recomputed. In the exterior of the film the charge density is given by a superposition of two-dimensional plane waves $S_{\vec{K}_{||}}(\vec{r})$,

$$\rho^{\mathrm{III}}(\vec{r}) = \sum_{\vec{K}_{||}} \rho_{\vec{K}_{||}}(z)\, S_{\vec{K}_{||}}(\vec{r}) \ . \tag{22}$$

For $d/2 \leq |z| \leq z_N$ $\rho^{\mathrm{III}}_{\vec{K}_{||}}(z)$ consists of piecewise polynomials up to degree 6. Again their amplitudes are found by summing over the $\vec{k}$ of the irreducible wedge and the different bands according to their occupancy. As a result of Eq. (13) $\rho_{\vec{K}}(z)$ decreases exponentially for $|z| > z_N$.

D. The effective potential

Within the Hohenberg-Kohn-Sham formalism[30] the effective potential is given by a sum of the electrostatic potential U and the exchange-correlation potential $V_{\mathrm{XC}}(\vec{r}) = \delta E_{\mathrm{XC}}[\rho]/\delta\rho(\vec{r})$ with the exchange-correlation energy E_{XC} of the electron gas with density $\rho(\vec{r})$. Although the electrostatic charge density looks the same as that given by Wimmer *et al.*[14] we use a different strategy to evaluate the electrostatic potential by adapting the method described by one of us[23] to slab geometry. Following this idea the total charge, which includes the contribution of the nuclei of charge Z^{μ} given by

$$\rho^{\mathrm{nuc}}(\vec{r}) = \sum_{\mu=-(N-1)/2}^{(N-1)/2} \sum_{\vec{R}_{||}} Z^{\mu}\delta(\vec{r} - \vec{R}^{\mu} - \vec{R}_{||}), \tag{23}$$

is decomposed into the terms

$$\rho(\vec{r}) + \rho^{\mathrm{nuc}}(\vec{r}) = \rho^{\mathrm{I}}(\vec{r}) + \tilde{\rho}^{\mathrm{II}}(\vec{r}) + \rho^{\mathrm{III}}(\vec{r}) + \rho^{K}(z) + \rho^{\mathrm{Ewald}}(\vec{r}), \tag{24}$$

which are all treated separately. $\vec{R}_{||}$ represents the vectors of the two-dimensional lattice. $\tilde{\rho}^{\mathrm{II}}(\vec{r})$ is obtained from $\rho^{\mathrm{II}}(\vec{r})$ by subtracting the point charge within each MT sphere,

$$q^{\mu} \equiv \int_{|\vec{r}-\vec{R}^{\mu}|<r^{\mu}_{\mathrm{APW}}} \rho^{\mathrm{II}}(\vec{r})d^3r = 4\pi \int_0^{r^{\mu}_{\mathrm{APW}}} \rho^{\mu}_0(r)\, r^2 dr, \tag{25}$$

as well as all higher multipole moments assumed to be situated at $\vec{R}^{\mu}$

$$q^{\mu}_l \equiv 4\pi \int_0^{r^{\mu}_{\mathrm{APW}}} \rho^{\mu}_l(r)\, r^{2+1} dr. \tag{26}$$

$\rho^{K}(z)$ is a homogeneous charge located at both boundaries of the layer chosen in such a way that the total charge due to ρ^{I}, ρ^{III}, and ρ^{K} vanishes within the elementary column:

$$\int_{\mathrm{I,II,III}} \left[\rho^{\mathrm{I}}(\vec{r}) + \rho^{\mathrm{III}}(\vec{r}) + \rho^{K}(z)\right] d^3r = 0. \tag{27}$$

ρ^{Ewald} describes the charge density of the nuclei and compensating charges and multipole moments.

$$\rho^{\mathrm{Ewald}}(\vec{r}) = \sum_{\mu=-(N-1)/2}^{(N-1)/2} \sum_{\vec{R}} \left[-Z^{\mu} + q^{\mu}_0 + \sum_{l=1} q^{\mu}_l D_l\right] \times\delta(\vec{r} - \vec{R}^{\mu} - \vec{R}) - \rho^{K}(z). \tag{28}$$

D_l is a differential operator with respect to the components of vectors $\vec{r}$,

$$D_l = \sum_{\nu_1}\sum_{\nu_2}\sum_{\nu_3} \alpha_{\nu_1\nu_2\nu_3} \frac{\partial^{\nu_1}}{\partial x_1^{\nu_1}} \frac{\partial^{\nu_2}}{\partial x_2^{\nu_2}} \frac{\partial^{\nu_3}}{\partial x_3^{\nu_3}} \delta_{\nu_1+\nu_2+\nu_3,l}, \tag{29}$$

where the $\alpha_{\nu_1\nu_2\nu_3}$ are chosen in such a way that D_l is invariant against the symmetry operations of the point group,

$$r^{l+1} D_l \frac{1}{r} = K_l(\vec{r}^{\,0}). \tag{30}$$

As a consequence of the above definition the mean value of $\rho^{\mathrm{Ewald}}(\vec{r})$ over the elementary column vanishes.

1. *The Coulomb potential due to $\rho^{\mathrm{I}} + \rho^{\mathrm{III}} + \rho^{K}$*

Due to the planar symmetry the corresponding electrostatic potential V^{C} can be expressed by a superposi-

tion of two-dimensional plane waves invariant under the group of point symmetry operations mapping the slab into itself.

$$V^C(\vec{r}) = \sum_{\vec{K}_{||}} V^C(\vec{K}_{||}, z)\, S_{\vec{K}_{||}}(z), \tag{31}$$

where $V^C(\vec{K}_{||}, z)$ is defined by the inhomogeneous differential equation

$$\left(\frac{\partial^2}{\partial z^2} - \vec{K}_{||}^2\right) V^C(\vec{K}_{||}, z) = -4\pi e^2 \left[\rho^{\mathrm{I}}_{\vec{K}_{||}}(z) + \rho^{\mathrm{III}}_{\vec{K}_{||}}(z) + \rho_0^K(Z)\delta_{\vec{k}}\right], \tag{32}$$

which may easily be solved with the appropriate boundary conditions for $|z| \longrightarrow \infty$. As a result of the small number of two-dimensional plane waves in the ansatz Eq. (5) the series (31) is rapidly convergent.

2. The Coulomb potential due to $\tilde{\rho}^{\mathrm{II}}$

As all multipole moments of the charge density $\tilde{\rho}^{\mathrm{II}}$ vanish, this potential reads within the MT sphere situated at $\vec{R}_{||} + \vec{R}^{\mu}$

$$\tilde{V}^{\mathrm{II}}(\vec{r}) = \sum_{l}^{2L} \sum_{m} \frac{4\pi e^2}{2l+1} K_{lm}(\vec{r}_0') \left\{ \frac{1}{r'^{l+1}} \int_0^{r'} \tilde{\rho}^{\mu}_{lm}(r'')\, r''^{2+l} dr'' + r'^{l} \int_{r'}^{r^{\mu}_{\mathrm{APW}}} \tilde{\rho}^{\mu}_{lm}(r'')\, r''^{1-l} dr'' \right\},$$

$$\vec{r}' = \vec{r} - \vec{R}_{||} - \vec{R}^{\mu}\ , \tag{33}$$

and is zero for $r' = |\,\vec{r} - \vec{R}_{||} - \vec{R}^{\mu}\,| \geq r^{\mu}_{\mathrm{APW}}$.

3. The contribution due to ρ^{Ewald}

It is suitable to treat the influence of the zero multipole contribution of Eq. (28)

$$\rho_0^{\mathrm{Ewald}}(\vec{r}) = \sum_{\mu=-(N-1)/2}^{(N-1)/2} \sum_{\vec{R}_{||}} (-Z^{\mu} + q^{\mu}) \times \delta(\vec{r} - \vec{R}^{\mu} - \vec{R}_{||}) - \rho^K(z) \tag{34}$$

separately. Outside the slab the corresponding potential $V_0^{\mathrm{Ewald}}(\vec{r})$ may easily be expressed by the Fourier series

$$V_0^{\mathrm{Ewald}}(\vec{r}) = \sum_{\vec{K}_{||}} e^{i\vec{K}_{||}\cdot\vec{r}_{||}}\, V^{\mathrm{Ewald}}_{0,\vec{K}_{||}}(z), \tag{35}$$

where

$$V^{\mathrm{Ewald}}_{0,\vec{K}_{||}}(z) = \begin{cases} 0, & \vec{K}_{||} = \vec{0} \\ \dfrac{2\pi e^2}{A|\,\vec{K}_{||}\,|} \sum_{\mu=-(N-1)/2}^{(N-1)/2} (-Z^{\mu} + q^{\mu})\, e^{-i\vec{K}_{||}\cdot\vec{R}^{\mu}} e^{-K_{||}|\,z - R^{\mu}_z|}, & \vec{K}_{||} \neq \vec{0}\ . \end{cases} \tag{36}$$

A denotes the area of the mesh spanned by the vectors $\vec{a}_1$ and $\vec{a}_2$, and R^{μ}_z the third component of $\vec{R}^{\mu}$. Due to the factor $e^{-K_{||}|\,z-R^{\mu}_z|}$ this Fourier series is rapidly convergent apart from the planes where the nuclei are located. Therefore inside the slab an adaption of Ewald's method to the slab geometry has been used. This is obtained from Eq. (B14) of Ref. 34 by integrating over the z component of $\vec{k}$ from $-\infty$ to ∞ using formula 3.954 of Ref. 35. Then $V_0^{\mathrm{Ewald}}(\vec{r})$ is expressed by a sum over both two-dimensional lattice vectors and reciprocal lattice vectors, both of which are absolutely convergent.

$$V_0^{\mathrm{Ewald}}(\vec{r}) = e^2 \sum_{\mu=-(N-1)/2}^{(N-1)/2} \sum_{\vec{R}_{||}} (-Z^{\mu} + q^{\mu}) \left[\frac{\mathrm{erfc}(\eta\,|\,\vec{r} - \vec{R}_{||} - \vec{R}^{\mu}\,|)}{|\,\vec{r} - \vec{R}_{||} - \vec{R}^{\mu}\,|}\right] + \sum_{\vec{K}_{||}} e^{i\vec{K}_{||}\cdot\vec{r}_{||}}\, \tilde{V}^{\mathrm{Ewald}}_{0,\vec{K}_{||}}(z), \tag{37}$$

where

$$\widetilde{V}^{\mathrm{Ewald}}_{0,\vec{K}_{||}}(z) = \begin{cases} -\frac{2\pi e^2}{A}\left(\sum_{\mu=-(N-1)/2}^{(N-1)/2}(-Z^\mu+q^\mu)\left[z_\mu\,\mathrm{erf}(\eta z_\mu)+\frac{e^{-\eta^2 z_\mu^2}}{\sqrt{\pi}\eta}\right]-q\,\frac{d}{2}\right), & \vec{K}_{||}=0 \\ \frac{\pi e^2}{AK_{||}}\sum_{\mu=-(N-1)/2}^{(N-1)/2}(-Z^\mu+q^\mu)\left[\mathrm{erfc}\left(\eta z_\mu+\frac{K_{||}}{2\eta}\right)e^{K_{||}z_\mu}\right. & \\ \qquad\left.+\mathrm{erfc}\left(-\eta z_\mu+\frac{K_{||}}{2\eta}\right)e^{-K_{||}z_\mu}\right]e^{-i\vec{K}_{||}\cdot\vec{R}^\mu}, & \vec{K}_{||}\neq 0\,, \end{cases} \tag{38}$$

$$z_\mu = z - \vec{R}^\mu_z.$$

In Eqs. (37) and (38) erf and erfc are the error function and the complementary error function, respectively and q denotes the charge of the compensating charge density ρ^K. By a proper choice of the parameter η a rapid convergence of both sums in Eq. (37) is achieved. In the MAPW scheme as in all other APW schemes it is advantageous that the first sum in Eq. (37) is a superposition of spherically symmetric potentials. An angular decomposition of the second sum may be obtained by adapting the strategy of Ref. 36 to the slab geometry. The multipole moments q_l^μ, $\mu = -(N-1)/2, (N-1)/2$, located at the lattice sites of the slab produce the potential

$$V_l^{\mathrm{Ewald}}(\vec{r}) = e^2 \sum_{\mu=-(N-1)/2}^{(N-1)/2}\sum_{\vec{R}_{||}} q_l^\mu \frac{K_{lm}[(\vec{r}-\vec{R}_{||}-\vec{R}^\mu)^0]}{|\,\vec{r}-\vec{R}_{||}-\vec{R}^\mu\,|^{l+1}}\,. \tag{39}$$

Even in the case of the fcc (100) surface all terms with $l \geq 1$ are nonzero. For small values of l the sum over the different lattice vectors is slowly convergent if it is convergent at all. Again, this difficulty can be overcome by an extension of the Ewald method to multipoles as was done by Kornfeld.[37] It is based on the fact that the potential V_l^{Ewald} is alternatively given by

$$V_l^{\mathrm{Ewald}}(\vec{r}) = e^2 \sum_{\mu=-(N-1)/2}^{(N-1)/2}\sum_{\vec{R}_{||}} q_l^\mu D_l \frac{1}{|\,\vec{r}-\vec{R}_{||}-\vec{R}^\mu\,|} \tag{40}$$

with the differential operator introduced in Eq. (29). Thus we have only to apply D_l to the potential produced by monopoles situated at the lattice points. But this potential is quite similar to the potential $V_0^{\mathrm{Ewald}}(\vec{r})$ treated above. As the corresponding expressions are quite lengthy we will not list them.

Finally the total electrostatic potential is given by

$$U(\vec{r}) = V^{\mathrm{c}}(\vec{r}) + \widetilde{V}^{\mathrm{II}}(\vec{r}) + \sum_{l=0}^{2L} V_l^{\mathrm{Ewald}}(\vec{r}) \tag{41}$$

with the asymptotic behavior

$$\lim_{|z|\to\infty} U(\vec{r}_{||}, z) = 0. \tag{42}$$

4. Exchange and correlation potential

For a given exchange-correlation potential v_{XC} this contribution to the effective potential can be calculated at any point of the slab by use of the charge density given in Sec. II C. The effective potential $V_{\mathrm{eff}}(\vec{r})$ for the self-consistent-field (SCF) calculation results from the sum of the exchange-correlation potential $v_{\mathrm{XC}}(\vec{r})$ and the total electrostatic potential $U(\vec{r})$.

E. The total energy

The Hohenberg-Kohn-Sham[30] formalism yields the total energy per unit column as a sum of band energies up to the Fermi energy E_F and the Coulomb energy of the nuclei at the atomic sites minus a term that corrects for double counting parts. Thereby, as was proven in Refs. 24 and 38, the infinite Coulomb energy of the electron and the infinite correction to the Coulomb energy of the electrons cancel each other exactly. Using this result we obtain in the LDA

$$\begin{aligned} E_0 = {} & 2\sum_{n,\vec{k}_{||}} E_{n\vec{k}_{||}}\,\Theta(E_F - E_{n\vec{k}_{||}}) - \frac{1}{2}\int \rho(\vec{r})\,V_{\mathrm{Coul}}(\vec{r})\,d^3r \\ & -\frac{1}{2}\sum_\mu Z^\mu \lim_{|\vec{r}-\vec{R}^\mu|\to 0}\left(e^2\frac{Z^\mu}{|\,\vec{r}-\vec{R}^\mu\,|}+V_{\mathrm{Coul}}(\vec{r})\right) \\ & +\int(\epsilon_{\mathrm{XC}}[\rho]-v_{\mathrm{XC}}[\rho])\,\rho(\vec{r})\,d^3r. \end{aligned} \tag{43}$$

Both integrals are to be extended over the unit column. The Coloumb potential $V_{\mathrm{Coul}}(\vec{r})$ is defined by

$$\begin{aligned} V_{\mathrm{Coul}}(\vec{r}) = {} & -e^2\sum_\mu\sum_{\vec{R}_{||}}\frac{Z^\mu}{|\,\vec{r}-\vec{R}-\vec{R}^\mu|} \\ & +e^2\int\frac{\rho(\vec{r}\,')}{|\,\vec{r}-\vec{r}\,'\,|}\,d^3r' \end{aligned} \tag{44}$$

and the exchange and correlation energy is approximated by

$$E_{\mathrm{XC}} = \int \rho(\vec{r})\,\epsilon_{\mathrm{XC}}[\rho(\vec{r})]\,d^3r, \tag{45}$$

where ϵ_{XC} is the exchange and correlation energy per volume of a uniform gas with $\rho(\vec{r})$ and

$$v_{\mathrm{XC}} = \epsilon_{\mathrm{XC}} + \rho\frac{d\epsilon_{\mathrm{XC}}}{d\rho}. \tag{46}$$

The evaluation of the various contributions of Eq. (43) follows closely the method described in Ref. 24. Besides the total energy the magnitudes of the kinetic energy T and of the Coulomb energy per unit column are rather interesting. As the Coulomb energy U is simply given by

$$U = \frac{1}{2}\int \rho(\vec{r})\, V_{\mathrm{Coul}}(r)\; d^3r - \sum_{\mu} Z^{\mu} \lim_{|\vec{r}-\vec{R}|\to 0}\left(e^2\frac{Z^{\mu}}{|\vec{r}-\vec{R}^{\mu}|} + V_{\mathrm{Coul}}(\vec{r})\right), \quad (47)$$

a direct evaluation of T can be avoided by use of the identity

$$E_0 = T + U + E_{\mathrm{XC}}. \quad (48)$$

III. COMPUTATIONAL DETAILS

The calculations were performed for Cu(100) films consisting of one, two, five, and seven layers. As a consequence of the odd number of layers, mirror symmetry with respect to the film normal does hold. Hence the wave functions must be either even or odd with respect to the $z \to -z$ transformation. No reconstruction of the film was assumed. That means that all MT spheres have the same radius $r_{\mathrm{APW}} = a/\sqrt{8} = 2.4152$ a.u.

A. The film-adapted MAPW band-structure calculation

In order to compare our results with previous SCF investigations[39] of the bulk we have chosen analoguous characteristics. That means four radial functions for $l = 0$ and $l = 1$ three radial functions for $l = 2$, and $L = 2$. Two-dimensional plane waves and the trigonometric functions defined by Eq. (3) are restricted by

$$|\vec{k} + \vec{K} + p_l\, \vec{e}_z\,|^2 \le \left(\frac{2\pi}{a}\right)^2 Q_{\max}, \quad Q_{\max} = 15.0. \quad (49)$$

In a monolayer this requirement allows up to 22 two-dimensional plane waves and six trigonometric functions. For thicker films the number of two-dimensional plane waves was kept the same whereas the number of trigonometric functions was increased as the p_l's decrease with the film width. $N = 9$ B splines outside the film boundary have been used with $|z_N - d/2| = 3r_{\mathrm{APW}}$. This guarantees the occupied states to be accurate at least up to 1 mRy. After elimination of the constraints the rank of the eigenvalue problem was 360, 400, 500, and 600, for the one-, three-, five-, and seven-layer films, respectively. The Fermi energy as well as the charge density were evaluated by an adaption of the Gilat-Raubenheimer-method[40,41] and the concept of special points[42–44] to layer problems. Within the irreducible mesh of the two-dimensional Brillouin zone 20 different $\vec{k}_{||}$ points were considered.

B. The effective potential

Inside the MT spheres the charge density was calculated in the form of a multipole and Fourier expansion, where angular moments greater then 12 were omitted in the multipole expansion. Following Moruzzi *et al.*[45] 129 quadratically spaced points

$$r_i = r_{\mathrm{APW}}(i-1)^2/128^2 \quad (50)$$

were assumed, which are also the break points of the spline interpolations. This grid was the basis for the evaluation of the Coulomb and the exchange-correlation potential, of the effective potential $V_{\mathrm{eff}}(\vec{r})$ and its Fourier coefficients $V_{\mathrm{eff}}(\vec{K}_{||})$, as well as the integrals contributing to E_0, E_{XC}, and U. Exchange and correlation energy were used in the parametrization of Hedin and Lundqvist[46] with the numerical parameters given by Gunnarson and Lundqvist.[47]

The present band-structure calculations were performed with a potential V_{eff} averaged over appropriately chosen directions which are found by generalizing the concept proposed by Bansil[48,49] and in Refs. 50 and 51. This simplifies not only the solution of the eigenvalue problem but also the evaluation of V^{Ewald} and $\tilde{V}^{II}$. We considered self-consistency achieved when the Fourier coefficients of V_{eff} changed by less than 10^{-8} from iteration to iteration. Then the iteration to iteration shift in total energy was less then $10\,\mu$ Ryd.

IV. RESULTS

A. Band structure

The energy band structure along the three high-symmetric lines $\bar{\Gamma}$-$\bar{X}$, $\bar{X}$-$\bar{M}$, and $\bar{M}$-$\bar{\Gamma}$ of the two-

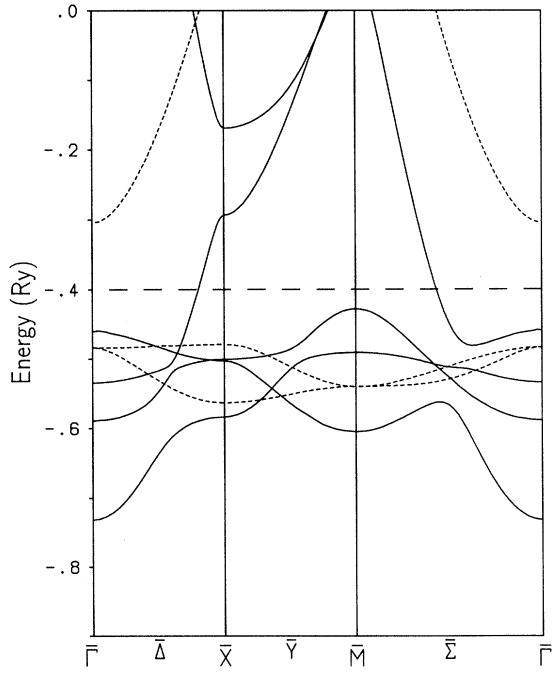

FIG. 2. Band structure for the Cu(001) monolayer along the symmetric lines in the two-dimensional Brillouin zone. Solid and dashed lines represent band structures which are even or odd, respectively, with respect to z reflection. The horizontal straight line shows the Fermi level.

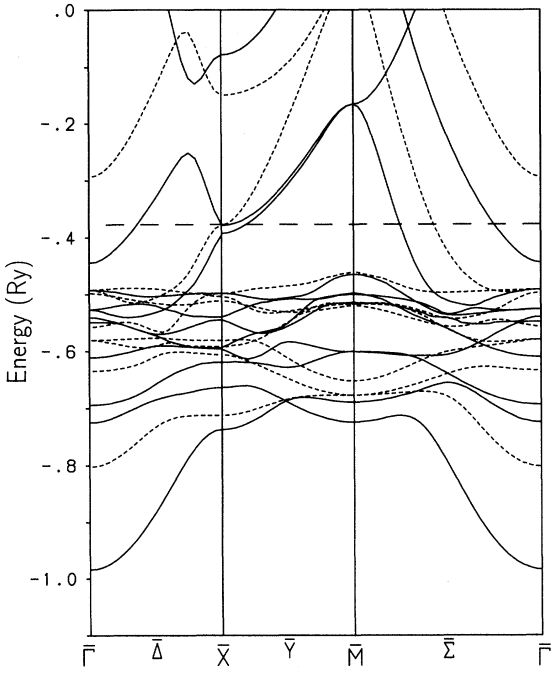

FIG. 3. Band structure for the Cu(001) three-layer film along symmetric lines in the two-dimensional Brillouin zone. Solid and dashed lines represent band structures which are, respectively, even or odd with respect to z reflection. The horizontal straight line shows the Fermi level.

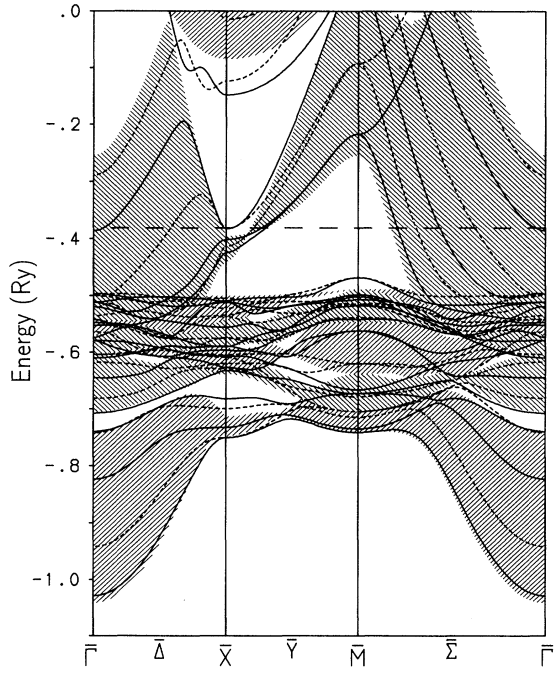

FIG. 4. Band structure for the Cu(001) five-layer film along the symmetric lines in the two-dimensional Brillouin zone. Solid and dashed lines represent band structures which are, respectively, even or odd with respect to z reflection. The horizontal straight line shows the Fermi level. Hatched regions represent the projected band structure.

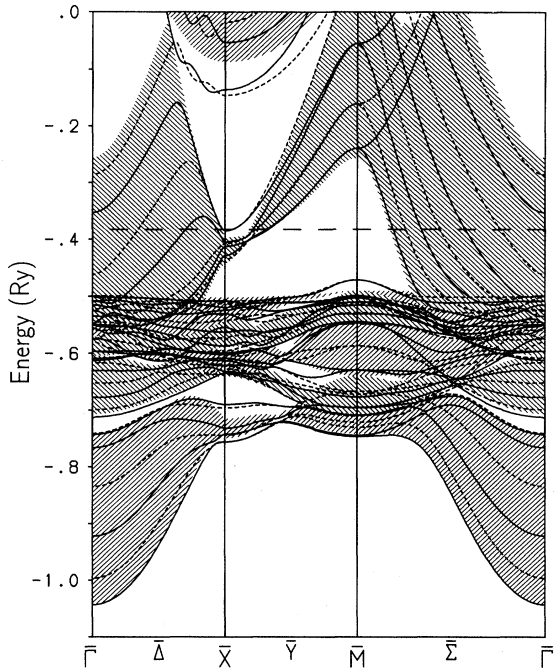

FIG. 5. Band structure for the Cu(001) seven-layer film along the symmetric lines in the two-dimensional Brillouin zone. Solid and dashed lines represent band structures which are, respectively, even or odd with respect to z reflection. The horizontal straight line shows the Fermi level. Hatched regions represent the projected band structure.

dimensional Brillouin zone is shown in Figs. 2–5 for the monolayer, three-layer, five-layer, and seven-layer Cu(100) slabs, respectively. Even states with respect to $z \rightarrow -z$ reflection are plotted by full lines, those with odd symmetry by broken lines. The horizontal dashed line marks the Fermi energy. Due to spin degeneracy, about 9.5 bands per layer below E_F are occupied, corresponding to 19 valence and higher core electrons. With increasing number of layers the various bands become closer and closer and we can imagine how they merge into a continuum in the limit of an infinite crystal. This limit is the projected band structure displayed by the hatching in Fig. 4 and Fig. 5. It was evaluated with the help of the MAPW scheme using a self-consistent potential with similar computational parameters as in the case of the layer problem. The white regions of the projected band structure denote energies which are not allowed in the bulk.

By comparing Fig. 4 and Fig. 5 we learn how the number of bands within the hatched regions increases, even and odd bands following each other almost equidistantly. As a result of their lower number of nodes the even bands are always energetically lower. It is remarkable that most of the bands obtained for seven layers are within the hatched regions and thus are allowed in the bulk. Bands or parts of bands in the white regions correspond to electronic states in the layer which may also appear in a semi-infinite crystal, as we shall see in the

next section.

Our result along $\overline{\Gamma}$-$\overline{M}$ illustrates clearly the hybridizing of an *sp* band with the *d* bands. On the basis of this picture we can conclude that the width of the *d* bands in the monolayer amounts to 200 mRy whereas it approaches the value of 300 mRy in the five- or seven-layer film, characteristic for the bulk. This narrowing of the *d* bands, also found in previous investigations,[2,5,8,20] is a result of the fact that in a monolayer the *d* functions are allowed to extend to the boundaries without any restriction.

The energy bands of the monolayer, Fig. 2, are overall quite similar in shape to the results of previous investigations.[20] However, in contrast to some older calculations,[5,7,9,52,53] all fully occupied bands are energetically more distant from the Fermi level. This is especially true for the third even occupied band at $\overline{M}$, which Krakauer *et al.*[8] and Smith and co-workers[2] locate quite close to the Fermi level. As in the recent work by Birkenheuer *et al.*[20] our calculations definitely exclude *d*-like hole states in the case of the Cu(100) monolayer. Finally, in the older calculations the parabolalike band of odd symmetry starting at -0.3 Ry is missing. All these difficulties may be a consequence of either the heuristic potentials used in the older calculations[4,52,53] or the specific choice of the basis set to describe the Bloch functions. Comparing with recent SCF investigations[2,5,20] quite good agreement is obtained. This is explicitly shown in Table II in which the energies at $\overline{\Gamma}$ and $\overline{M}$, relative to the Fermi energy, are compared with those obtained by Birkenheuer *et al.*[20] using the FILMS and FLAPW methods and by Wang and Freeman[5] using the self-consistent numerical basis set LCAO method.

In general the MAPW and FILMS method energies are quite close; some of them differ by less than 10 mRy and the biggest deviation amounts to 27 mRy, whereas the deviations from the FLAPW results are quite large. Roughly speaking the FILMS results are in between our energies and the FLAPW energies. This is quite remarkable since up to now the FLAPW scheme has been considered as a standard for high-precision studies of solid surfaces.[16] For the unoccupied states even greater differences occur. For example, the parabolalike band of even symmetry starts at $\overline{\Gamma}$ in the FILMS and FLAPW results, closer to the Fermi energy than in our case, whereas we find the second unoccupied state of even symmetry at $\overline{X}$ lower by 100 mRy than in the investigation of Birkenheuer *et al.*[20] The band structure of the seven-layer film displayed in Fig. 5 is in surprisingly good agreement with the highly accurate SCF LCGTO results of Euceda *et al.*[6]

TABLE II. Comparison of E_F and the valence band energies of the monolayer relative to E_F at $\overline{\Gamma}$ and $\overline{M}$ obtained by different methods.

	MAPW	FILMS[a]	FLAPW[a]	LCAO[b]
E_F	−0.400	−0.355	−0.328	−0.362
$E_{\overline{\Gamma}_1} - E_F$	−0.332	−0.338	−0.366	−0.357
$E_{\overline{\Gamma}_3} - E_F$	−0.189	−0.216	−0.235	
$E_{\overline{\Gamma}_1} - E_F$	−0.135	−0.142	−0.153	
$E_{\overline{\Gamma}_5} - E_F$	−0.083	−0.096	−0.106	
$E_{\overline{\Gamma}_4} - E_F$	−0.060	−0.083	−0.094	
$E_{\overline{M}_4} - E_F$	−0.205	−0.222	−0.235	−0.2087
$E_{\overline{M}_5} - E_F$	−0.140	−0.149	−0.163	
$E_{\overline{M}_1} - E_F$	−0.091	−0.098	−0.109	
$E_{\overline{M}_3} - E_F$	−0.028	−0.053	−0.062	−0.0213

[a]Reference 20.
[b]Reference 5.

B. Surface states

In a layer the definition of surface states is in some respects, arbitrary because there is no sharp distinction between original bulk states and new states created by the formation of the surface. By comparing the two-dimensional band structure obtained for an increasing number of layers with the projected band structure, possible surface states can be found. They are characterized by curves in the forbidden part of the projected band structure which remains quite stationary. In addition, surface states localized within the width of the layer manifest themselves by the fact that the curves of even and odd states come quite close. This is certainly not true for surface states having a quite long decay length in the semi-infinite medium. In the case of a seven-layer slab we observe such states located at $\overline{X}$ as well as at $\overline{M}$. At $\overline{X}$ there are three such doubly degenerate states located at 300 and 2.3 mRy below and 244 mRy above E_F, where even and odd states are separated by 10, 0.1, and 10 mRy, respectively. In all these cases these differences decrease with increasing number of layers, whereas the mean value of both energies remains stationary. On an enlarged scale the dispersion of the occupied state quite near the Fermi energy as well as the experimental results obtained by angle-resolved photoemission spectroscopy[54] are displayed in Fig. 6. Up to a constant shift of 2 mRy

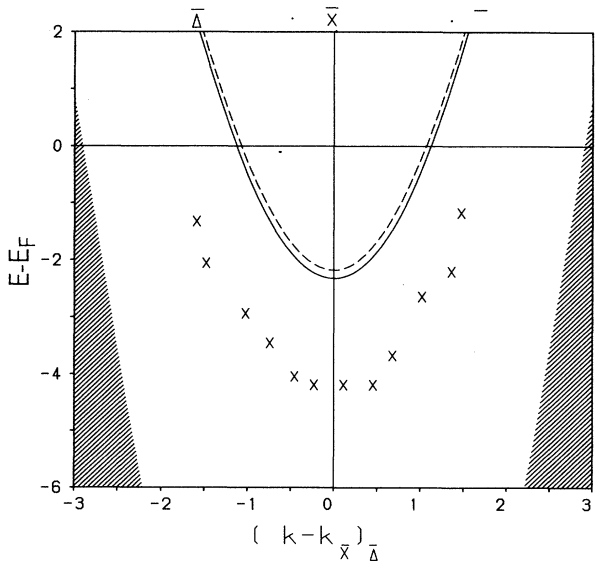

FIG. 6. Surface-state dispersion of the state $\overline{X}$ close to E_F. Solid and dashed curves are theoretical results for even or odd states, respectively. Crosses are experimental results (Ref. 54). The shaded curve is the projected bulk continuum. $(\vec{k} - \vec{k}_\Delta)_\Delta$ in units of $10^{-2} 2\pi/a$. $E - E_F$ in units of 10^{-3} Ry.

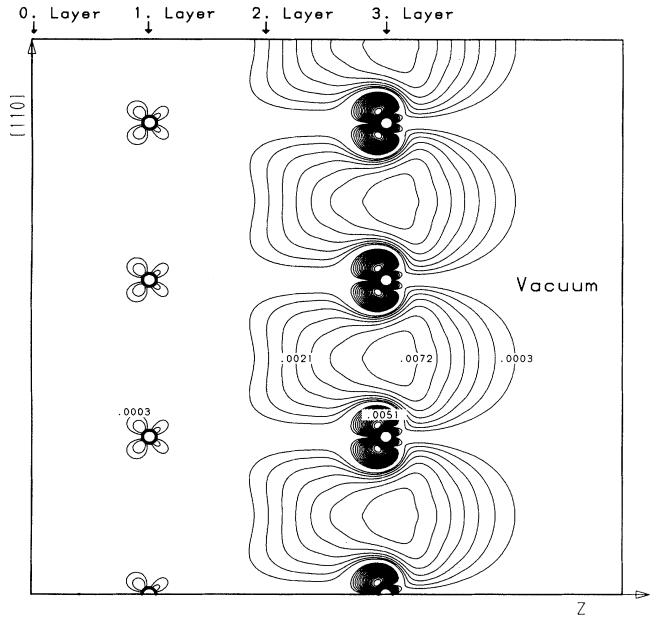

FIG. 7. Contour plot of the electronic charge density in the (110) plane of the surface state at $\overline{X}$. Each contour line differs by a factor proportional to ρ^3.

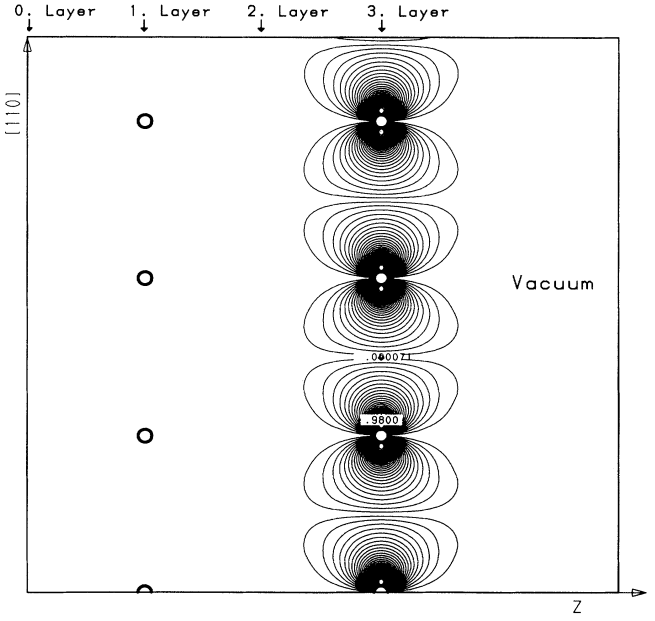

FIG. 9. Contour plot of the electronic charge density in the (110) plane of the surface state near $\overline{M}$ 80 mRy below E_F. Each contour line differs by a factor proportional to ρ^3.

theoretical and experimental results coincide. This excellent agreement is certainly due to the fact that in the LDA only the energies near E_F have a physical meaning. Figure 7 showing the contour of the electronic charge density is further evidence for a surface state as the charge density is only nonzero in the last two layers.

At $\overline{M}$ an almost degenerate state at 89 mRy below E_F is observed with an energy separation of even and odd states amounting to 17 μRy. Shifted by 40 mRy to lower energies, the corresponding dispersion curve agrees quite well with angle-resolved photoemission spectroscopy measurements[55] (see Fig. 8). As we learn from Fig. 9, showing again a contour plot of the electronic charge density, this state is completely localized in the last surface layer.

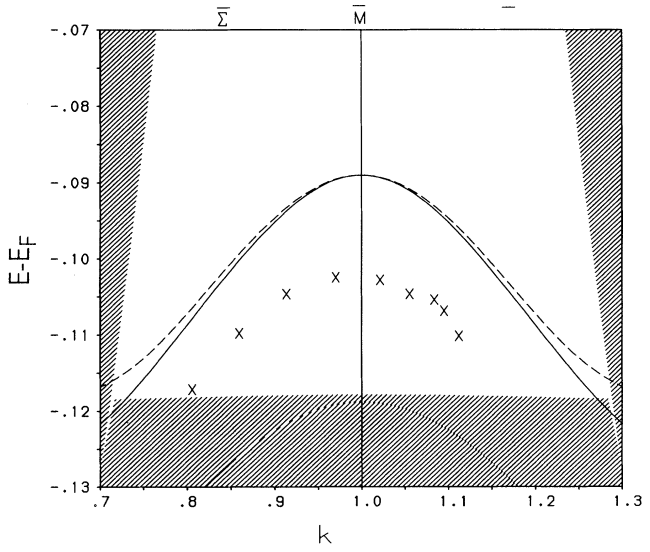

FIG. 8. Surface-state dispersion near $\overline{M}$ 80 mRy below E_F. Solid and dashed curves in the theoretical result for even or odd states, respectively. Crosses are experimental results (Ref. 55). The shaded curve is the projected bulk continuum. $|\vec{k}_\Sigma|$ in units of $2\pi/a$. $E - E_F$ in units of Ry.

C. Density of states

Once self-consistency was achieved the density of states was evaluated by use of 200 equally spaced $\vec{k}_{||}$ points within the irreducible wedge of the two-dimensional Brillouin zone to reduce unphysical structures. In Figs. 10–13 the density of states per volume is displayed for the four different layers considered. The dotted curves in Fig. 12 and Fig. 13 are of the same magnitude as for the bulk evaluated with similar computational parameters.

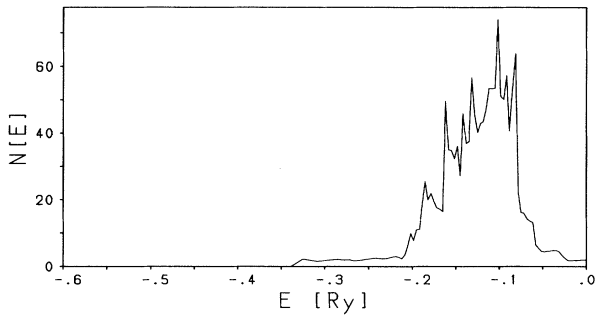

FIG. 10. Density of states for the Cu(001) monolayer.

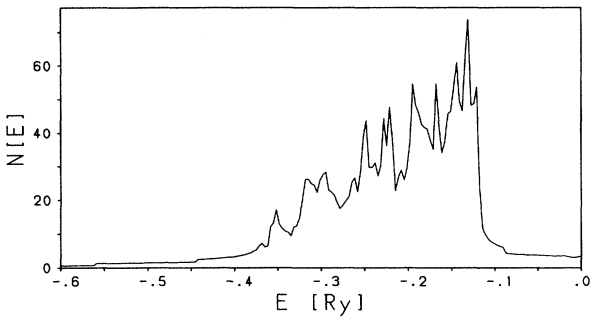

FIG. 11. Density of states for the Cu(001) three-layer film.

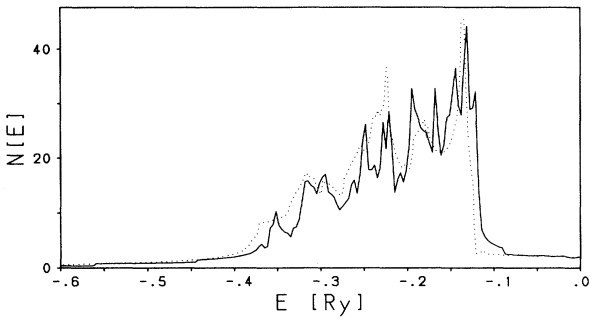

FIG. 12. Density of states for the Cu(001) five-layer film (full line) and for the bulk (dotted line).

Again we can see how the bulk behavior is approached asymptotically with increasing number of layers, starting with the three-layer slab. However, the monolayer shows a completely different behavior. First, the width of the occupied states is smaller by about 100 mRy than in other cases, as discussed in Sec. IV A. Secondly, for certain energies the curve of the density of states is discontinuous. This is a consequence of the reduction from three dimensions to two dimensions. Similar discontinuities show in the other $N(E)$ curves also, but their height is reduced as we have normalized $N(E)$ to unit volume. The discontinuity about 0.09 Ry below E_F is a typical example for such behavior. It is attributed to the surface states about $\overline{M}$ discussed in the last section.

D. Charge density and Coulomb potential

According to the LDA the charge density obtained by the self-consistent scheme has some physical relevance. Figure 14 is the electronic charge density map of a seven-layer Cu(001) film on the (110) plane for positive z values. Up to the top level the charge density is found to be only slightly different from its value in the bulk. Even in the top layer noticeable charges are seen outside the

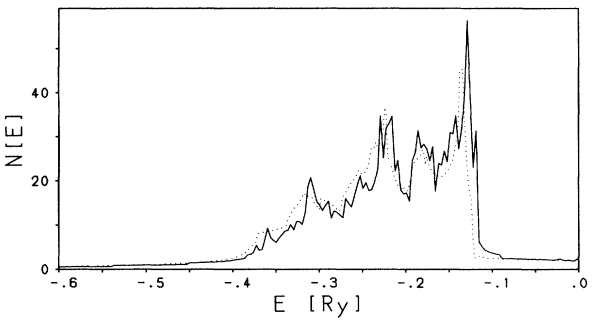

FIG. 13. Density of states for the Cu(001) seven-layer film (full line) and for the bulk (dotted line).

TABLE III. The work function of one-, three-, five-, and seven-layer Cu(100) films and of a semi-infinite Cu(100) crystal in units of eV.

Monolayer	5.442
Three layers	5.316
Five layers	5.180
Seven layers	5.209
LMTO-ASA[a]	5.26
Expt.[b]	5.155 ± 0.054
Expt.[c]	4.59 ± 0.054
Expt.[d]	5.10 ± 0.03
Expt.[e]	4.58, 4.76
Expt.[f]	4.77 ± 0.05

[a]Reference 26.
[b]Reference 60.
[c]Reference 61.
[d]Reference 62.
[e]Reference 63.
[f]Reference 64.

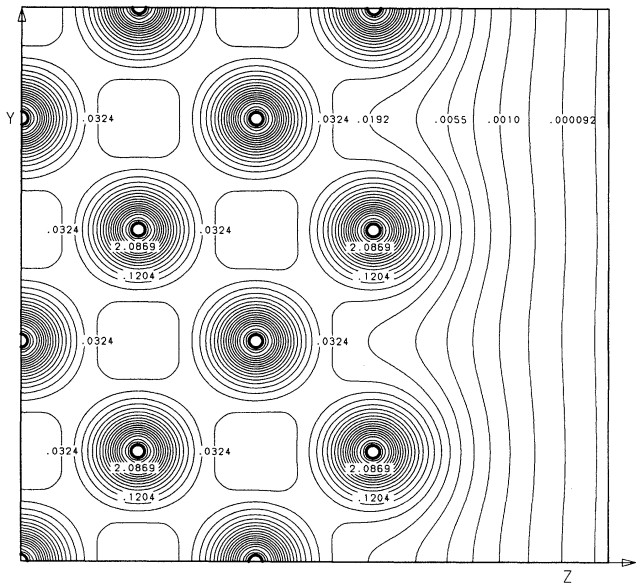

FIG. 14. Contour plot of the total electronic charge density in the (110) plane of the Cu(001) seven-layer film. Each contour line differs by a factor proportional to ρ^5.

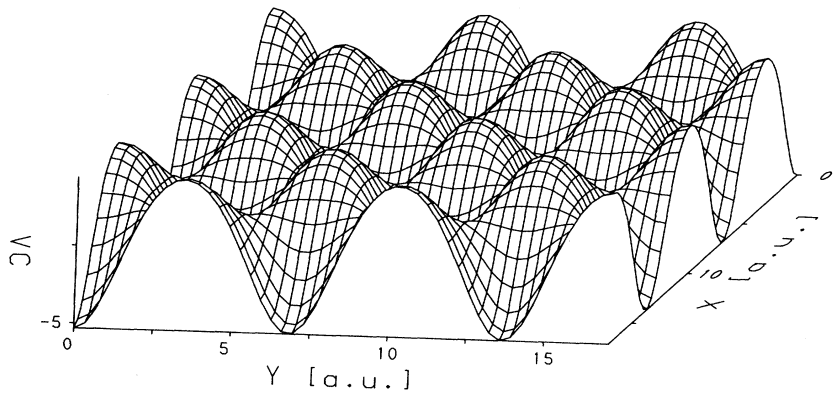

FIG. 15. Stereographic plot of the Coulomb potential outside the film in the plane having $a/2$ distance from the surface in units of 10^{-2} Ry.

atomic cores. There the charge density gradually approaches its zero value. Analogously to the uniform background model[56,57] a surface barrier is produced as some charges are leaking out of the hypothetically defined surface of the film. Similar results were obtained in other self-consistent calculations.[2,5] Finally, the stereographic plots of the Coulomb potential outside the film displayed in Figs. 15–17 are quite instructive. They show how the lateral variations of the potential produced by the nuclei of the uppermost layer rapidly smooth out with increasing distance from the film surface.

E. Work function

As we have chosen the potential to be zero far away from the film the work function is given according to Schulte[58,59] by

$$\Phi = -E_F \ . \tag{51}$$

Its values obtained for the four films of different thickness are listed in Table III together with the theoretical value obtained by use of the LMTO ASA Green's function technique[26] and various experimental results for the semi-infinite Cu(001) crystal.[60–64]

From our result we conclude that Φ approaches a value of about $5.20\,eV$ in an oscillating manner. It is slightly less than the LMTO atomic-sphere approximation (ASA) value and in good agreement with the experimental value quoted by Delchar[60] and Strayer *et al.*[62] However, at the moment it is not clear whether the other experimental values[61,63,64] are more reliable. In this case a potential without any shape restrictions is expected to bring Φ into better agreement with the experimental value as the surface barrier depends sensitively on the potential.

F. Total energy and surface energy

In Table IV the total energy, the kinetic energy, and the Coulomb energy per layer for the one-, three-, five-, and seven-layer films as well as for the bulk are listed. Again, it is remarkable how the total energy gradually approaches its bulk value. This is not the case for the Coulomb and kinetic energies as these quantities are not stationary in the LDA formalism.

In order to evaluate the surface energy E_s, i.e., the energy which is gained by the system because of the formation of the surface, we adopted the formalism described by Feibelman.[65] It is based on the assumption that adding layers to the slab just increases the total energy by adding energies of bulklike layers E_B and leaves the surface energy constant. Thus for a slab consisting of n layers the total energy is written as

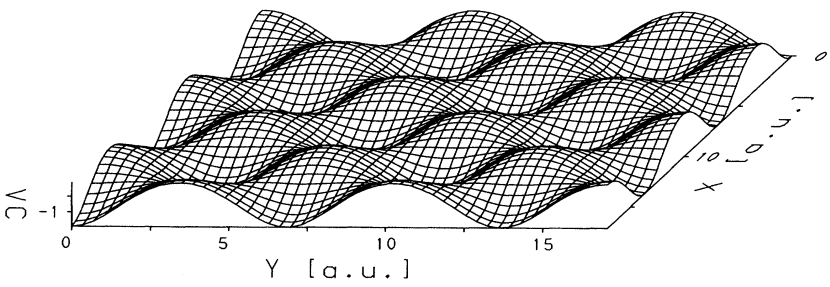

FIG. 16. Stereographic plot of the Coulomb potential outside the film in the plane having $5a/8$ distance from the surface in units of 10^{-2} Ry.

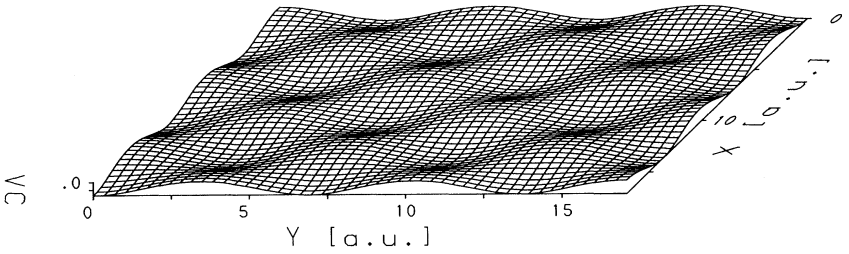

FIG. 17. Stereographic plot of the Coulomb potential outside the film in the plane having $3a/4$ distance from the surface in units of 10^{-3} Ry.

$$E_0(n) = 2E_S + nE_B \ . \tag{52}$$

Figure 18 showing the total energy for $n = 1$, 3, 5, and 7 verifies this assumption. By a least squares fit we obtain $E_B = -3277.025\,\mathrm{Ry}$ and $E_S = 0.0540\,\mathrm{Ry}$. E_B is found quite close to the value of $E_0(\infty)$ given in Table IV. Using a Green's function technique, based on the linear-muffin-orbitals method within the tight-binding and atomic-sphere approximation the value $E_S = 0.062$ eV has been obtained.[26] No experimental value of E_S is available for Cu(100).

G. Electric field gradient

Due to cubic symmetry all elements of the tensor of the electric field gradient vanish within the bulk. However, in the case of a fcc (100) layer the elements $V_{xx} = V_{yy}$ and V_{zz} are nonzero. In Table V the values of V_{zz} at the nuclei of the different layers of a seven-layer film are listed. As a result of the fact that the charge density aproaches its bulk value in the middle of the film the corresponding value of V_{zz} is quite small. However, in the top layer it is larger almost by a factor of 3 and of opposite sign. An experimental value of V_{zz} was found via nuclear quadrupole hyperfine interaction using perturbed $\gamma\gamma$ angular correlation spectroscopy.[66] After annealing at room temperature it was found that the iridium atoms deposited onto a Cu(115) surface occupy substitutional sites in the (100)-oriented terraces characterized by $|V_{zz}| = 9.0 \times 10^{17}$ V/cm^2. The same value was detected in annealing experiments on various vicinal copper surfaces with (001) terraces. Thus the theoretical value is too small by a factor of 3. We believe that this dicrepancy is a result of the fact that the nonspherical parts of the potential near the nuclei have been neglected. In other investigations[67] the field gradient was found to be quite sensitive to the shape restriction of the potential.

V. CONCLUSIONS

We have generalized the MAPW method to deal with thin films. The method has the advantage that it is computationally efficient and that by a proper choice of the numerical parameters any desired accuracy is achieved. The decomposition of the Bloch functions into direct-space and Fourier-space parts is quite useful for the evaluation of the self-consistent potential in the LDA.

Its application to the Cu(001) film with increasing number of layers demonstrates how the energy bands gradually fill up the allowed energy region of the projected band structure obtained with the same numerical parameters. Approximately doubly degenerate states of even and odd symmetry in the forbidden region are localized on both surfaces of the film and correspond to surface states of the semi-infinite crystal of the same surface structure. At $\overline{M}$ and $\overline{X}$ of a Cu(001) seven-layer film such states are found, which agrees well with experimental results.

From the similarity of the density of states curve and the charge density in the middle of the film with the corresponding magnitudes in the bulk it can be concluded that a seven-layer film is sufficiently thick to screen the effect of the two surfaces inside the slab and thus might be an appropriate model for a semi-infinite crystal. On

TABLE IV. The Coulomb energy U, the kinetic energy T, and the total energy E_0 per layer for the one-, three-, five-, and seven-layer films and the bulk.

	One layer	Three layers	Five layers	Seven layers	Bulk
U	−6419.462	−6420.293	−6419.853	−6419.883	−6419.295
T	3272.508	3273.437	3272.947	3272.980	3272.329
E_0	−3276.913	−3276.926	−3276.995	−3277.002	−3277.048

TABLE V. The value of the component of the tensor of electric field gradient in the different layers of a seven-layer film in units of 10^{17} V/cm^2.

	V_{zz} (10^{17} V/cm^2)
Layer 0	0.822
Layer 1	0.429
Layer 2	0.338
Layer 3	−2.793

the vacuum sides of the top layer both magnitudes are considerably different from their bulk values.

More accurate investigations without shape restrictions of the potential are necessary to bring the leading components of the tensor of the electric field gradient into better agreement with recent experimental results. Due to experimental uncertainties it is not clear whether such corrections are also necessary to explain the experimental value of the work function.

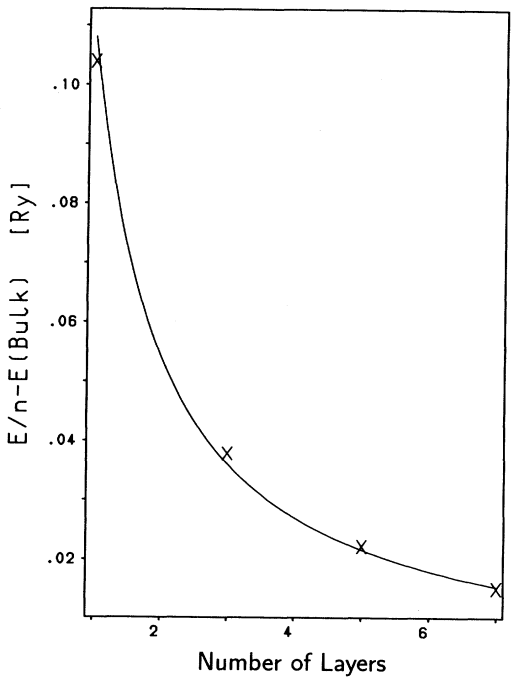

FIG. 18. The total energy E_F as a function of the number of layers.

ACKNOWLEDGMENTS

The investigations described in this publication were performed when one of us (H.B.) was at the Department of Physics, Montana State University in Bozeman. He gratefully acknowledges the kind hospitality and especially thanks Professor J. Hermanson for his continuous interest.

[1] K.-M. Ho, B. N. Harmon, and S. H. Liu, Phys. Rev. Lett. **44**, 1531 (1980); D. M. Kolb, W. Boeck, K.-M. Ho, and S. H. Liu, *ibid.* **47**, 1921 (1981); K.-M. Ho and K. P. Bohnen, *ibid.* **59**, 1833 (1987).
[2] J. G. Gay, J. R. Smith, and F. J. Arlinghaus, Phys. Rev. Lett. **38**, 561 (1977); J. R. Smith, J. G. Gay, and F. J. Arlinghaus, Phys. Rev. B **21**, 2201 (1980); **21**, 2201 (1980); J. R. Smith, F. J. Arlinghaus, and J. G. Gay, *ibid.* **22**, 4757 (1980); F. J. Arlinghaus, J. G. Gay, and J. R. Smith, *ibid.* **20**, 1332 (1979); **23**, 5152 (1981).
[3] P. J. Feibelmann, Phys. Rev. B **26**, 5347 (1982).
[4] K. S. Sohn, D. G. Dempsey, L. Kleinman, and Ed. Caruthers, Phys. Rev. B **13**, 1515 (1976).
[5] C. S. Wang and A. J. Freeman, Phys. Rev. B **18**, 1714 (1978); **19**, 793 (1979).
[6] A. Euceda, D. M. Bylander, L. Kleinman, and K. Mednick, Phys. Rev. B **27**, 659 (1983).
[7] O. Jepsen, J. Madsen, and O. K. Andersen, Phys. Rev. B **18**, 605 (1978).
[8] H. Krakauer, M. Posternak, and A. J. Freeman, Phys. Rev. B **19**, 1706 (1979).
[9] M. Posternak, H. Krakauer, A. J. Freeman, and D. D. Koelling, Phys. Rev. B **21**, 5601 (1980).
[10] D. R. Hamann, L. F. Matheiss, and H. S. Greenside, Phys. Rev. B **24**, 6151 (1981).
[11] D. S. Wang, A. J. Freeman, and H. Krakauer, Phys. Rev. B **26**, 1340 (1982).
[12] O. Jepsen, J. Madsen, and O. K. Andersen, Phys. Rev. B **26**, 2790 (1982).
[13] L. F. Matheiss and D. R. Haman, Phys. Rev. B **29**, 5372 (1984).
[14] E. Wimmer, H. Krakauer, M. Weinert, and A. J. Freeman, Phys. Rev. B **24**, 864 (1981).
[15] S. Ohnishi, A. J. Freeman, M. Weinert, and K. Mednick, Phys. Rev. B **28**, 6741 (1983).
[16] H. Erschbaumer, A. J. Freeman, C. L. Fu, and R. Podloucky, Surf. Sci. **243**, 317 (1991).
[17] J. W. Mintmire, J. R. Sabin, and S. B. Trickey, Phys. Rev. B **26**, 1743 (1982).
[18] J. C. Boettger and S. B. Trickey, J. Phys. Condens. Matter **1**, 4323 (1989).
[19] G. W. Fernando, B. R. Cooper, M. V. Ramana, H. Krakauer, and C. Q. Ma, Phys. Rev. Lett. **56**, 2299 (1986).
[20] U. Birkenheuer, N. Rösch, S. B. Trickey, and J. Noffke, Z. Phys. B **83**, 267 (1991).
[21] H. Bross, Phys. Kondens. Matter **3**, 119 (1964).
[22] H. Bross, G. Bohn, G. Meister, W. Schubö, and H. Stöhr, Phys. Rev. B **2**, 3098 (1970).
[23] H. Bross and R. Eder, Phys. Status Solidi B **144**, 175 (1987).
[24] H. Bross and R. Stryczek, Phys. Status Solidi B **144**, 675 (1987).
[25] J. E. Inglesfield and G. A. Benesh, Phys. Rev. B **37**, 6682 (1988).
[26] H. L. Skriver and N. M. Rosengaard, Phys. Rev. B **46**, 7157 (1992).
[27] J. A. Appelbaum and D. R. Hamann, Phys. Rev. B **6**, 2166 (1972).
[28] E. Hahn, Ph.D. thesis, Munich University, 1989.
[29] W. Hummel, Ph.D. thesis, Munich University, 1995.

[30] P. Hohenberg and W. Kohn, Phys. Rev. **136**, B864 (1964); W. Kohn and L. J. Sham, *ibid.* **140**, A1133 (1965); L. J. Sham and W. Kohn, *ibid.* **145**, 561 (1966).
[31] C. de Boor, *A Practical Guide to Splines* (Springer, New York, 1978); J. Stoer and R. Bulirsch, *Introduction to Numerical Analysis* (Springer, New York, 1980); H. Hämmerlin and K. H. Hoffmann, *Numerische Mathematik* (Springer, Berlin 1989).
[32] M. Kauzmann, Ph.D. thesis, Munich University, 1994.
[33] G. F. Koster, in *Solid State Physics: Advances in Research and Applications*, edited by F. Seitz and D. Turnbull (Academic Press, New York, 1957), Vol. 5, p. 173
[34] C. Kittel, *Introduction to Solid State Physics,* 1st ed. (J. Wiley and Sons, New York, 1953).
[35] I. S. Gradshteyn and I. M. Ryzhik, *Table of Integrals, Series and Products* (Academic Press, New York, 1980).
[36] G. M. Fehrenbach and H. Bross, Phys. Rev. B **48**, 17 703 (1993).
[37] H. Kornfeld, Z. Phys. **22**, 27 (1924).
[38] M. Weinert, E. W. Wimmer, and A. J. Freeman, Phys. Rev. B **26**, 4571 (1982)
[39] H. Bross (unpublished).
[40] G. Gilat and L. J. Raubenheimer, Phys. Rev. **144**, 390 (1966); L. J. Raubenheimer and G. Gilat, *ibid.* **157**, 586 (1967); G. Gilat, Phys. Rev. B **26**, 2243 (1982).
[41] H. Bross, Phys. Status Solidi B **179**, 429 (1993).
[42] D. J. Chadi and M. L. Cohen, Phys. Rev. B **8**, 5747 (1973); D. J. Chadi, *ibid.* **16**, 1746 (1977).
[43] H. J. Monkhorst and J. D. Pack, Phys. Rev. B **13**, 5188 (1976).
[44] H. Bross, J. Phys. F **8**, 2631 (1978).
[45] V. L. Moruzzi, J. F. Janak, and A. R. Williams, *Calculated Electronic Properties of Metals* (Pergamon Press, New York, 1978).
[46] L. Hedin and B. I. Lundqvist, J. Phys. C **4**, 2064 (1971).
[47] O. Gunnarson and B. I. Lundqvist, Phys. Rev. B **13**, 4274 (1976).
[48] A. Bansil, Solid State Commun. **16**, 885 (1975).
[49] R. Prasal and A. Bansil, Phys. Rev. B **21**, 496 (1980).
[50] W. R. Fehlner and S. H. Vosko, Can. J. Phys. **54**, 2159 (1976).
[51] W. R. Fehlner, S. B. Nickerson, and S. H. Vosko, Solid State Commun. **19**, 83 (1976).
[52] B. R. Cooper, Phys. Rev. Lett **30**, 1316 (1973); Phys. Rev. B **16**, 5595 (1977).
[53] G. S. Painter, Phys. Rev. B **17**, 3848 (1978); **18**, 955 (1978).
[54] S. D. Kevan, Phys. Rev. B **28**, 2268 (1983).
[55] P. Heimann, J. Hermanson, H. Miosga, and H. Neddermeyer, Phys. Rev. Lett. **42**, 1782 (1979); Phys. Rev. B **20**, 3059 (1979).
[56] N. D. Lang and W. Kohn, Phys. Rev. B **1**, 4555 (1970); **3**, 1215 (1971).
[57] N. D. Lang, in *Solid State Physics: Advances in Research and Applications*, edited by F. Seitz, D. Turnbull, and H. Ehrenreich (Academic Press, New York, 1973), Vol. 28, p. 225.
[58] F. K. Schulte, J. Phys. C **7**, L370 (1974); Surf. Sci. **55**, 427 (1976); Z. Phys. B **27**, 303 (1977).
[59] F. K. Schulte and J. Hölzl, Surf. Sci. **85**, 4 (1979).
[60] T. A. Delchar, Surf. Sci. **27**, 11 (1971).
[61] P. O. Gartland, S. Berge, and B. J. Slagsvold, Phys. Rev. Lett. **28**, 738 (1972).
[62] R. W. Strayer, W. Macki, and L. W. Swanson, Surf. Sci. **34**, 225 (1973).
[63] G. A. Haas and R. E. Thomas, J. Appl. Phys. **48**, 86 (1977).
[64] G. G. Tibbets, J. M. Burkstrand, and J. C. Tracy, Phys. Rev. B **15**, 3652 (1977).
[65] P. J. Feibelman, Phys. Rev. B **27**, 1991 (1983).
[66] R. Fink, G. Krausch, B. Luckscheiter, P. Platzer, U. Wöhrmann, and G. Schatz, Phys. Rev. Lett. **70**, 2455 (1993).
[67] P. Blaha and K. H. Schwarz, J. Phys. F **17**, 899 (1987).